COMMUNICATION

A Nitrogen-Rich 2D sp^2 Carbon-Linked Conjugated Polymer Framework as a High-Performance Cathode for Lithium-ion Batteries

Shunqi Xu,[#] [a] Gang Wang,[#] [a] Bishnu P. Biswal,[‡] [a] Matthew Addicoat,[▽] [b] Silvia Paasch,[c] Wenbo Sheng,[d] Xiaodong Zhuang,[a] Eike Brunner,[c] Thomas Heine,[b] Reinhard Berger,*[a] Xinliang Feng*[a]

Abstract: In this work, we report a novel two-dimensional (2D) sp^2 carbon-linked conjugated polymer framework (2D CCP-HATN) with a nitrogen-doped skeleton, a periodical dual-pore structure and high chemical stability. The chemical identity of the polymer backbone consisting of hexaazatrinaphthalene (HATN) and cyanovinylene units linked entirely by carbon-carbon double bonds is verified by FT-IR, Raman and solid-state ^{13}C cross-polarization magic-angle spinning (CP-MAS) NMR spectroscopies. In stacked form, together with the imine-linked covalent organic framework analogue 2D C=N HATN, the interior framework architecture of the crystalline 2D CCP-HATN is unambiguously demonstrated by powder X-ray diffraction and N_2 adsorption-desorption measurements. Profiting from the shape-persistent framework of 2D CCP-HATN integrated with the electrochemical redox-active HATN and the robust sp^2 carbon-carbon linkage, 2D CCP-HATN hybridized with carbon nanotubes shows a high capacity of 116 mA h/g, with high utilization of its redox-active sites and superb cycling stability (91% after 1000 cycles) and rate capability (82%, 1.0 A/g vs 0.1 A/g) as an organic cathode material for lithium-ion batteries.

Two-dimensional (2D) conjugated polymers with tailorable repeat units have attracted increasing attention due to their precise and predictable structures, which make them promising for meeting different specific requirements by ingenious designs.[1-5] In particular, the incorporation of redox-active building blocks into robust 2D conjugated polymer frameworks is highly promising for energy storage applications because of the following merits:[6-7, 23-25] 1) the porous and layered structure can provide transport pathways for both ions and electrons along the stacking directions and within the layers, and 2) the shape-persistent framework structure guarantees high chemical and electrochemical stabilities, which are particularly important for long-term operation at the accelerated current densities. Nevertheless, a main challenge remains in confining suitable redox-active building blocks into stable 2D conjugated polymer frameworks. Thus far, the construction of 2D conjugated polymer frameworks has been mainly driven by imine-linked covalent organic frameworks (COFs),[8] π-conjugated metal-organic frameworks (MOFs),[9] covalent triazine frameworks (CTFs),[10] etc.[11-13] However, the stability issues of imine-based COFs[13] and MOFs and the harsh reaction conditions needed for synthesizing 2D CTFs[10] hamper their wide application.

Recently, we reported the first construction of a 2D sp^2-carbon-linked conjugated polymer (2D CCP) framework with a hexagonal structure through the Knoevenagel condensation reaction (Figure 1b).[2] Jiang et al. demonstrated the interesting magnetic properties of such 2D CCPs.[3] Compared with the aforementioned 2D conjugated polymer frameworks, 2D CCPs are of interest in terms of their high chemical stability and enhanced delocalized electronic structures. However, the synthesis of 2D CCPs remains challenging, as sp^2 carbon bond formation suffers from lower reversibility and therefore likely produces kinetically controlled amorphous porous polymers.[2,3,14-15] Until now, the construction of 2D CCPs with heteroatom-doped skeletons, which allow tuning of the redox behavior and can be applied in energy storage, has not yet been explored due to the synthetic difficulties mentioned above.

In this work, we demonstrate a novel 2D CPP by incorporating the nitrogen-rich hexaazatrinaphthalene (HATN) derivative [16] as a symmetrically rigid planar monomer with an excellent conjugated aromatic system and multiple redox-active properties. A starburst-shaped HATN-based monomer, namely, 2,3,8,9,14,15-hexa(4-formylphenyl)diquinoxalino[2,3-a:2',3'-c]phenazine (HATN-6CHO, Figure 1a), was thus synthesized and polymerized with 1,4-phenylenediacetonitrile (PDAN) via a base-catalyzed Knoevaenagel condensation reaction into a 2D CCP framework (2D CCP-HATN, Figure 1a). The corresponding imine-linked COF analogue of 2D CCPs with a comparable powder X-ray diffraction (PXRD) pattern due to their close unit-cell size, namely, 2D C=N HATN (Figure 1a), was also synthesized. Their interior structures were unambiguously disclosed by simulated and experimental PXRD patterns, as well as N_2 adsorption-desorption measurements. Benefiting from the nature of sp^2 carbon-carbon linkages, the 2D CCP-HATN exhibited superb chemical and electrochemical stabilities. Furthermore, after enhancing the conductivity of 2D CCP-HATN by in situ growth on carbon nanotubes (CNTs),[6] the resultant 2D CCP-HATN@CNT core-shell hybrids demonstrated a high capacity of 116 mA h/g and high utilization of redox-active units (HATN), with superb

[a] S. Xu, Dr. G. Wang, Dr. B. P. Biswal, Dr. X. Zhuang, Dr. R. Beger, Prof. X. Feng
Center for Advancing Electronics Dresden (cfaed) and Department of Chemistry and Food Chemistry, Dresden University of Technology,
Mommsenstrasse 4, 01069, Dresden, Germany
E-mail: xinliang.feng@tu-dresden.de
reinhard.berger@tu-dresden.de
[b] Dr. M. Addicoat, Prof. T. Heine
Wilhelm-Ostwald-Institute for Physical and Theoretical Chemistry, Leipzig University
Linnéstrasse 2, 04103 Leipzig, Germany
[c] Dr. S. Paasch, Prof. E. Brunner.
Chair of Bioanalytical Chemistry, Technische Universität Dresden, 01062, Dresden, Germany.
[d] W. Sheng
Chair of Macromolecular Chemistry, School of Science, Dresden University of Technology, Mommsenstrasse 4, 01069, Dresden, Germany
[#] These authors contributed equally.
[‡] Present address: Max-Planck-Institute for Solid State Re-search, Heisenbergstraße 1, 70569 Stuttgart, Germany.
[▽] Present address: School of Science and Technology, Notting-ham Trent University, Clifton Lane, Nottingham, NG11 8NS, UK

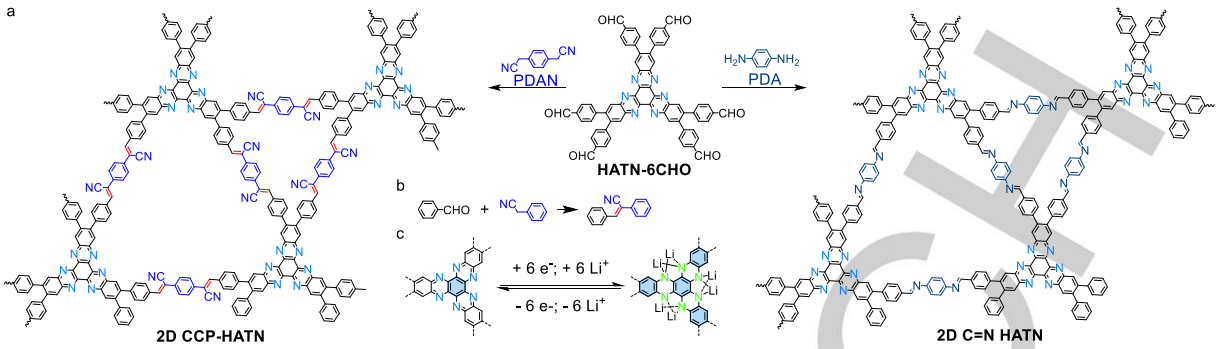

Figure 1. a) Scheme for the synthesis of 2D CCP-HATN and 2D C=N HATN from HATN-6CHO; b) Knoevenagel condensation reaction for sp^2 carbon linkage formation; c) Proposed Li storage behavior of the redox-active unit in 2D CCP-HATN.

cycling stability (91% capacity retention after 1000 cycles) and rate capability (82%, 1.0 A/g vs 0.1 A/g) as a cathode material for lithium-ion batteries (LIBs).

Since the Knoevenagel condensation reaction has a low reversibility, the formation of crystalline 2D CCPs is generally challenging. A comprehensive screening of over 30 solvothermal synthesis conditions was carried out (see section B in SI). Because of the good solubility of the linker PDAN, the combination of polar/good solvents (dimethylacetamide (DMAc), N-methy1-2-pyrrolidon) with nonpolar/poor solvents (mesitylene, 1,2-dichlorobenzene (*o*-DCB)) for the HATN-6CHO with a specific ratio is necessary to obtain crystalline 2D CCP-HATN. The reason could be that the dissolving rate of the monomers and the polymerization and precipitation rates can affect the kinetics of condensation and crystal growth by controlling the solubility of HATN-6CHO and the polarity of the solvents.[17] The detailed optimized conditions are provided in the Supporting Information. Thus, the crystalline 2D CCP-HATN was prepared via an optimized reaction by heating 1 eq. HATN-6CHO (12 mg, 0.012 mmol) and 3 eq. PDAN (5.6 mg, 0.037 mmol) in a mixture of DMAc (0.5 mL), *o*-DCB (0.5 mL) and Cs_2CO_3 (3 eq.12.01 mg, 0.037 mmol) as a base in a sealed glass ampoule at 120 °C for 3 days, affording the targeted 2D CCP-HATN in 91% yield.

The efficient linkage formations within the 2D CCP-HATN and 2D C=N HATN were further confirmed by FT-IR and solid-state ^{13}C-(CP-MAS) NMR spectroscopy. In the FT-IR spectrum of 2D CCP-HATN (Figure S1), the disappearance of absorption around 2824 and 2730 cm^{-1} (CHO groups) and the shift in the absorption of -CN groups from 2250 to 2217 cm^{-1} (C=C-CN) manifest a high degree of polymerization and a negligible contribution from unreacted groups (Figure S2 for 2D C=N HATN). In the solid-state ^{13}C-NMR spectra (Figure 2a and 2b). The chemical shift of ~157 ppm in 2D C=N HATN and ~110 ppm in 2D CCP-HATN can be assigned to the formation of imine linkages and carbon-carbon double bonds, respectively. The chemical stability was investigated by immersing the samples into various solvents for one week. Both 2D CCP-HATN and 2D C=N HATN showed high stability in organic solvents according to the PXRD data analysis (Figure S16-17); however, when immersed in acid/base solutions, the 2D CCP-HATN maintained high stability, whereas the 2D C=N HATN mostly dissolved in the concentrated HCl solution (Figure S18).

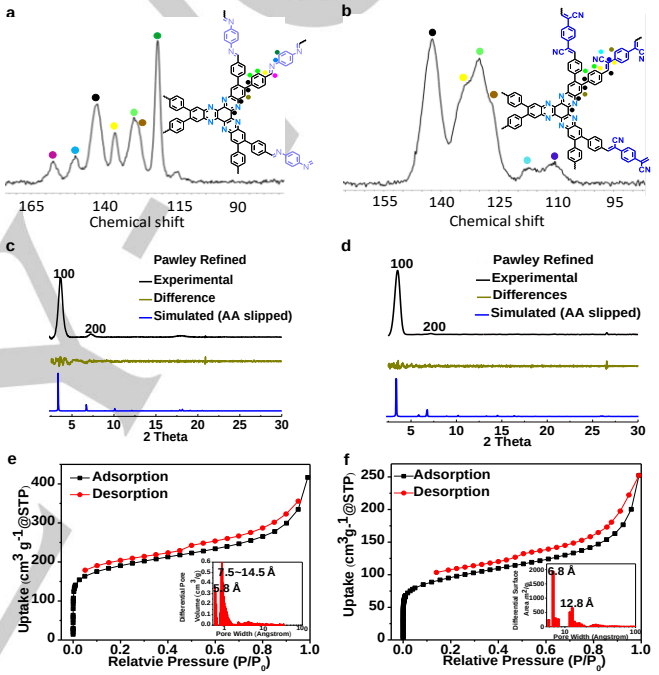

Figure 2. Solid-state ^{13}C-NMR spectra of (a) 2D C=N HATN and (b) 2D CCP-HATN; Experimental, Pawley-refined and simulated PXRD patterns and difference plots for (c) 2D C=N HATN and (d) 2D CCP-HATN; N_2 adsorption-desorption isotherms and pore-size distributions of (e) 2D C=N HATN and (f) 2D CCP-HATN.

Together with 2D C=N HATN, the crystallinity and interior architecture of the bulk powders of 2D CCP-HATN were investigated by experimental and simulated PXRD patterns (Figure 2c, 2d). Both experimental PXRD profiles exhibit reflections at 3.55° and 7.12°, which can be assigned to (100) and (200) planes, respectively, indicating long-range ordering in the two 2D polymer frameworks. Both 2D conjugated polymer framework models were optimized using the density functional tight binding method (DFTB$^+$).[18-19] From the optimized monolayer structures, three stacking modes were investigated, namely, eclipsed (AA), staggered (AB) and slipped AA stacking. Both 2D C=N HATN and 2D CCP-HATN were found to adopt slipped AA stacking, with per-layer stabilization energies of 77.6 and 97.0 kcal/mol, respectively (Table S2-3). These optimized structures were further used for the Pawley refinement in the Reflex module

of BIOVIA Materials Studio 2017 (Figure 2c, 2d). The calculated lattice parameters are a = 28.9416(±0.2), b = 28.0252 (±0.2), c = 7.3685 (±0.05), α = 87.6776 (±0.04), β = 77.8097 (±0.05) and γ = 118.59102 (±0.07), with R_{wp} = 2.74% and R_p = 9% for 2D C=N HATN, and a = 27.6365, b = 29.6446, c = 7.4535, α = 93.38098 (±0.03), β = 76.2396 (±0.02) and γ = 114.4051 (±0.03), with R_{wp} = 2.73% and R_p = 8.73% for 2D CCP-HATN (One unit-cell contains two layers). The difference plots also show that the refined diffraction patterns are consistent with the experimental PXRD data.

N_2 adsorption-desorption measurements were performed at 77 K to elucidate the porosity and further confirm the stacking model of the 2D C=N HATN and 2D CCP-HATN. As shown in Figure 2e and 2f, the isotherm plots of both 2D C=N HATN and 2D CCP-HATN displayed a sharp rise in the low-pressure range (P/Po=0~0.01), which can be assigned to a type I nitrogen sorption isotherm, indicating a microporous character. The Brunauer-Emmett-Teller (BET) surface areas of 2D C=N HATN and 2D CCP-HATN, calculated in the range of P/P_o=0.01-0.3 (Figure S14-15), are 670 and 317 cm^2/g, respectively. The nonlocal density functional theory (NLDFT) was applied to calculate the pore size distributions, and the results showed two main pore size distributions: ~5.8 Å and 7.5~14 Å for 2D C=N HATN and ~6.8 Å and ~12.8 Å for 2D CCP-HATN, which are smaller than the theoretical values calculated from the AA stacking model of 8 Å and 16 Å (Figure S13). This result can be attributed to the slipped stacking models. Thereby, together with 2D C=N HATN, the above N_2 adsorption-desorption measurement as well as the experimental and simulated PXRD patterns clearly demonstrate the formation of a dual-pore structure for the 2D CCP-HATN.

Considering the well-defined channels along the stacking direction, fully conjugated structures and shape-persistent framework in the 2D CCP frameworks, which can facilitate fast ion diffusion and suppress the dissolution of redox-active centers, we envision that the robust 2D CCP-HATN containing HATN units could serve as sustainable organic cathodes for lithium-ion batteries (Figure 1c). Toward this end, the electrochemical behavior of 2D CCP-HATN for LIBs was investigated in a potential window of 1.2-3.9 V in coin cells, where Li foil acted as the counter electrode and 1.0 M LiTFSI in 1,3-dioxolane and dimethoxyethane acted as the electrolyte. The cyclic voltammetry (CV) curve of 2D CCP-HATN showed four distinct redox peaks at 1.60/1.58 V and 2.45/2.4 V (vs Li/Li+, Figure 3c), indicating that the HATN embedded in the 2D CCP-HATN functions well as a redox-active center to reversibly store Li ions[26]. In contrast, 2D C=N HATN displayed much more vague redox bands, which suggested the superior redox properties of 2D CCP-HATN over 2D C=N HATN. The charge storage capability of 2D CCP-HATN for LIBs was further evaluated under a galvanostatic charge-discharge test at a current density of 0.1 A/g. The pure 2D CCP-HATN delivered a limited capacity of 62.5 mA h/g (Figure S27), which is much lower than its theoretical value of 117 mA h/g (Figure S24-25) and corresponds to 53% utilization of the redox-active sites. The reason for such low utilization can be assigned to the deeply buried active sites inside the stacked polymer frameworks and the low intrinsic electrical conductivity of 2D CCP-HATN ($9.1*10^{-10}$ S/cm, Figure S22, see section L in SI).[6]

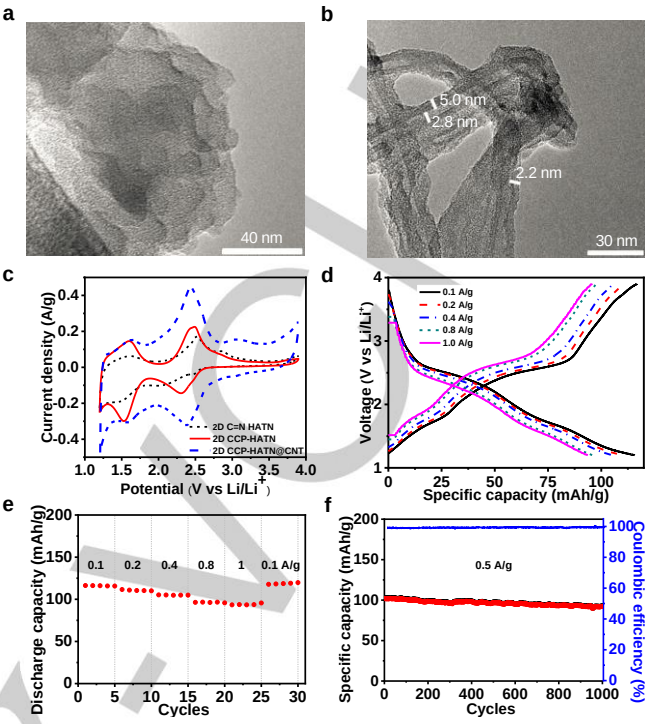

Figure 3. TEM images of (a) 2D CCP-HATN and (b) 2D CCP-HATN@CNT. (c) CV curve of 2D C=N HATN, 2D CCP-HATN and 2D CCP-HATN at a scan rate of 1 mV/s. (d) Charge-discharge profiles and (e) rate capability of 2D CCP-HATN@CNT at different current densities. (f) Cycling performance of 2D CCP-HATN@CNT at 0.5 A/g.

To expose the redox-active sites and enhance the electrical conductivity, the 2D CCP-HATN was directly grown in situ (see details in SI) on the surface of CNTs during the solvothermal reaction and was named as 2D CCP-HATN@CNT.[6] The PXRD patterns (Figure S19) together with SEM images (Figures S20-21) showed that when the amount of CNT was optimized to 50%, the 2D CCP-HATN could be uniformly coated on the CNTs while maintaining the crystallinity. The TEM image further revealed the interesting core-shell structure [20] of 2D CCP-HATN@CNT, with an average thickness of ~2.8 nm (Figure 3a-b), corresponding to ~7 layers of the 2D CCP-HATN shell. In addition, the resultant hybrid 2D CCP-HATN@CNT (with 50% CNT) exhibited an electrical conductivity of 0.4 S/cm (Figure S23), which is several orders higher than that of pristine 2D CCP-HATN. For the CV measurement, 2D CCP-HATN@CNT demonstrated similar but profound redox peaks and a larger CV area than did the pure 2D CCP-HATN, indicating a similar charge storage mechanism yet a higher active site utilization (Figure 3c). As shown in Figure 3d, 2D CCP-HATN@CNT also presented symmetrical charge-discharge curves, highlighting the high reversibility of the electrochemical redox process. Remarkably, the stable capacity of 2D CCP-HATN in the 2D CCP-HATN@CNT hybrid was largely enhanced to 116 mA h/g, with a much higher utilization of redox-active sites (HATN) (the capacity of CNTs is only 31 mA h/g, Figure S26) with 73% utilization, which is much higher than that of the pristine 2D CCP-HATN.

Additionally, 2D CCP-HATN@CNT showed an excellent rate capability. Upon increasing the current rates from 0.1 to 1 A/g, the charge-discharge curves maintained a similar shape with

negligible polarization (Figure 3d), representing fast electrochemical reaction kinetics. Even at 1.0 A/g, a high capacity of 94 mA h/g could be retained, corresponding to 81% of its value at 0.1 A/g (Figure 3e). Furthermore, the 2D CCP-HATN@CNT hybrid exhibited outstanding long-term cycling stability (Figure 3f), with 91% capacity retention after 1000 cycles at 0.5 A/g, which is higher than those of the most recently reported HATN-containing materials (Table S4). The average Coulombic efficiency for 2D CCP-HATN@CNT was as high as 99.3%. The high-performance origin of 2D CCP-HATN@CNT could be assigned to the following merits: 1) the shape-persistent sp^2 carbon-conjugated frameworks with high electrochemical stability; 2) the unique core-shell structure of the hybrid, with CNT providing the electron transport pathway and the exposed shell delivering active sites[20]; and 3) a surface-controlled pseudocapacitive process (see Section M in SI), which was further elucidated by impedance spectra (Figure S29) and CV measurements (Figure S30-31).[21,22]

In summary, we report a novel sp^2 carbon-linked conjugated 2D polymer framework with a nitrogen-doped skeleton and a dual-pore structure. The strong sp^2 carbon linkages and persistent framework render the resultant 2D CCP-HATN with high chemical and electrochemical stabilities. Furthermore, the open channels of the robust conjugated frameworks together with the high electrical conductivity of CNTs make the 2D CCP-HATN@CNT hybrid an excellent cathode material for LIB, with high utilization of redox-active sites, cycling-stability and rate capability. This work enriches the family of sp^2 carbon-linked 2D conjugated polymer frameworks, which paves the way for the future design and synthesis of novel 2D CCPs with expanded application scopes in organic electronics, energy storage and conversion, etc.

Acknowledgements

We thank the financial support from the European Union's Horizon 2020 research and innovation program under grant agreement No 696656 (Graphene Flagship Core2), Coordination Networks: Building Blocks for Functional Systems (SPP 1928, COORNET), the Center for Advancing Electronics Dresden (cfaed), the European Social Fund, and the Federal State of Saxony (ESF-Project "GRAPHD", TU Dresden. X.Z. thanks the financial support from NSFC (51722304, 21720102002, 5171101862). We thank Dr. Tao Zhang, Dr. Kun Xu and Dr. Junzhi Liu, for helpful discussions. We thank Dr. Philipp Schlender for PXRD measurements. We thank Dr. Petr Formanek (Leibniz Institute for Polymer Research, IPF, Dresden) for the TEM measurements.

Keywords: 2D conjugated polymer framework• sp^2-carbon-linked conjugated• high stability

[1] S. Lin, C. S. Diercks, Y.-B. Zhang, N. Kornienko, E. M. Nichols, Y. Zhao, A. R. Paris, D. Kim, P. Yang, O. M. Yaghi, C. J. Chang, *Science*. **2015**, *349*, 1208.

[2] X. Zhuang, W. Zhao, F. Zhang, Y. Cao, F. Liu, S. Bi, X. Feng, *Polym. Chem*. **2016**, *7*, 4176–4181.

[3] E. Jin, M. Asada, Q. Xu, S. Dalapati, M. A. Addicoat, M. A. Brady, H. Xu, T. Nakamura, T. Heine, Q. Chen, D. Jiang, *Science*. **2017**, *357*, 673–676.

[4] H. Xu, S. Tao, D. Jiang, *Nat. Mater*. **2016**, *15*, 722–726.

[5] G. Fiori, F. Bonaccorso, G. Iannaccone, T. Palacios, D. Neumaier, A. Seabaugh, S. K. Banerjee, L. Colombo, *Nature Nanotech*, **2014**, *9*, 768–779.

[6] F. Xu, S. Jin, H. Zhong, D. Wu, X. Yang, X. Chen, H. Wei, R. Fu, D. Jiang, *Sci. Rep*. **2015**, *5*, 8225.

[7] A. Halder, M. Ghosh, A. Khayum M, S. Bera, M. Addicoat, H. S. Sasmal, S. Karak, S. Kurungot, R. Banerjee, *J. Am. Chem. Soc*. **2018**, *140*, 10941–10945.

[8] Y.Jin, Y. Hu, W.Zhang, *Nat. Rev. Chem*. **2017**,*1*, 0056.

[9] R. Dong, Z. Zhang, D. C. Tranca, S. Zhou, M. Wang, P. Adler, Z. Liao, F. Liu, Y. Sun, W. Shi, Z. Zhang, E. Zschech, S. C.B. Mannsfeld, C. Felser, X. Feng, *Nat. Commun*. **2018**, *9*, 2637.

[10] P.Kuhn. M. Antonietti. A. Thomas, *Angew. Chem. Int. Ed*. **2008**, *47*, 3450 –3453.

[11] J. Guo, Y. Xu, S.Jin, L. Chen, T. Kaji, Y. Honsho, M. A. Addicoat, J. Kim, A. Saeki, H. Ihee, S. Seki, S. Irle, M. Hiramoto, J. Gao, D. Jiang, *Nat. Commun*. **2013**, *4*, 2736.

[12] P. J. Waller, Y. S. AlFaraj, C. S. Diercks, N. N. Jarenwattananon, O. M. Yaghi, *J. Am. Chem. Soc*, **2018**, *140*, 9099-9103.

[13] F. Haase, E. Troschke, G. Savasci, T. Banerjee, V. Duppel, S. Dörfler, M. M.J. Grundei, A. M. Burow, C. Ochsenfeld, S. Kaskel, B.V. Lotsch, *Nat. Commun*. **2018**, *9*, 2600.

[14] A. Yassin, M. Trunk, F. Czerny, P. Fayon, A. Trewin, J. Schmidt, A. Thomas, *Adv. Funct. Mater*. **2017**,*27*, 1700233.

[15] S. Shimizu, S. Shirakawa, T.Suzuki, Y. Sasaki, *Tetrahedron*. **2001**, *57*, 6169-6173

[16] J. L. Segura, R. Juárez, M. Ramos, C. Seoanea, *Chem. Soc. Rev*., **2015**, *44*, 6850—6885.

[17] X. Ding, J. Guo, X. Feng, Y. Honsho, J. Guo, S. Seki, P. Maitarad, A. Saeki, S. Nagase, D. Jiang, *Angew. Chem. Int. Ed*. **2011**, *50*, 1289 –1293

[18] B. Aradi, B. Hourahine, Th. Frauenheim, *J. Phys. Chem. A*, **2007**, *111*, 5678–5684.

[19] M. Elstner, D. Porezag, G. Jungnickel, J. Elsner, M. Haugk, Th. Frauenheim, S. Suhai, and G. Seifert, *Phys. Rev. B*, **1998**, *58*, 7260.

[20] X. Zhuang, F. Zhang, D. Wu, N. Forler, H. Liang, M. Wagner, D. Gehrig, M. R. Hansen, F. Laquai, X. Feng, *Angew. Chem. Int. Ed*. **2013**, *52*, 9668 –9672

[21] V. Augustyn, J. Come, M. A. Lowe, J. W. Kim, P.-L. Taberna, S. H. Tolbert, H. D. Abruña, P. Simon, B. Dunn, *Nat. Mater*. **2013**, *12*, 518-522.

[22] G. Wang, M. Yu, J. Wang, D. Li, D. Tan, M. Löffler, X. Zhuang, K. Müllen, X. Feng, *Adv. Mater*, **2018**, 1800533.

[23] J. Xie, P. Gu, Q. Zhang, *ACS Energy Lett*. **2017**, *2*, 1985−1996

[24] X. Zhan, Z. Chen, Q. Zhang, *J. Mater. Chem. A*. **2017**, *5*, 14463– 14479.

[25] Z.-Q. Lin, J. Xie, B.-W. Zhang, J.-W. Li, J. Weng, R.-B. Song, X. Huang, H. Zhang, H. Li, Y. Liu, Z. J. Xu, W. Huang, Q. Zhang. *Nano Energy*. **2017**, 41, 117-127.

[26] C. Peng, G.-H. Ning, J. Su, G. Zhong, W. Tang, B. Tian, C. Su, D. Yu, L. Zu, J. Yang, M.-F. Ng, Y.-S. Hu, Y. Yang, M. Armand, K. P. Loh, *Nature Energy*, **2017**, 17074.

COMMUNICATION

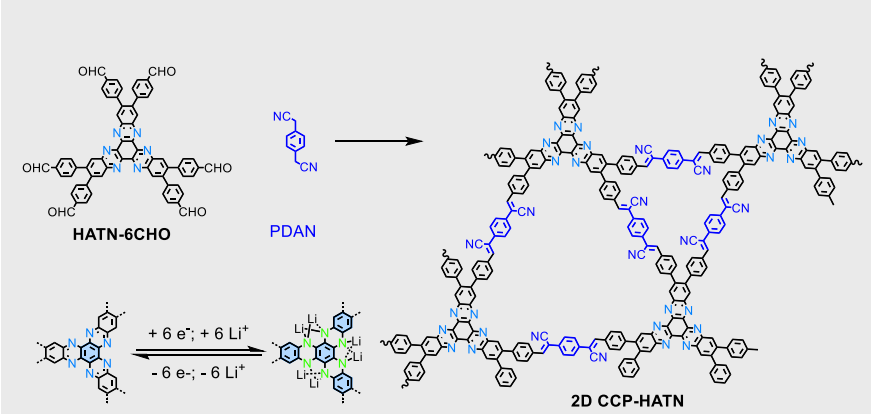

Shunqi Xu,[#a] Gang Wang,[#a] Bishnu P. Biswal,[‡a] Matthew Addicoat,[▽b] Silvia Paasch,[c] Wenbo Sheng,[d] Xiaodong Zhuang,[a] Eike Brunner,[c] Thomas Heine,[b] Reinhard Berger,[a] Xinliang Feng*[a]*

Page No. – Page No.

A Nitrogen-Rich 2D sp2 Carbon-Linked Conjugated Polymer Framework as a High-Performance Cathode for Lithium-ion Batteries

A 2D sp^2-carbon-linked conjugated polymer (2D CCP) framework with nitrogen-doped skeleton and multiple redox-active sites as organic cathode for lithium-ion battery.